Title

Rho GTPases and the Downstream Effectors Actin-related Protein 2/3 (Arp2/3) Complex and Myosin II Induce Membrane Fusion at Self-contacts*

Journal

Journal of Biological Chemistry, 290(6)

ISSN

0021-9258

Authors

Sumida, Grant M

Yamada, Soichiro

Publication Date

2015-02-01

DOI

10.1074/jbc.m114.612168

THE JOURNAL OF BIOLOGICAL CHEMISTRY VOL. 290, NO. 6, pp. 3238–3247, February 6, 2015

Rho GTPases and the Downstream Effectors Actin-related Protein 2/3 (Arp2/3) Complex and Myosin II Induce Membrane Fusion at Self-contacts*[S]

Received for publication, September 15, 2014, and in revised form, December 15, 2014 Published, JBC Papers in Press, December 19, 2014, DOI 10.1074/jbc.M114.612168

Grant M. Sumida and Soichiro Yamada[1]

From the Department of Biomedical Engineering, University of California, Davis, California 95616

Background: Normal epithelial cells remove self-junctions through membrane fusion.
Results: Self-contact induced membrane fusion is regulated by Rho GTPases via myosin II and the Arp2/3 complex.
Conclusion: Self-contact-induced membrane fusion requires Arp2/3 activity to bring membranes into close apposition to fuse.
Significance: Understanding fusion between self-contacting membranes provides a mechanistic template for membrane fusion such as cell-to-cell fusion and phagocytosis.

Actin regulation is required for membrane activities that drive cell adhesion and migration. The Rho GTPase family plays critical roles in actin and membrane dynamics; however, the roles of the Rho GTPase family are not limited to cell adhesion and migration. Using micron-sized obstacles to induce the formation of self-contacts in epithelial cells, we previously showed that self-adhesion is distinct from cell-to-cell adhesion in that self-contacts are eliminated by membrane fusion. In the current study, we identified Rho GTPases, RhoA, Rac1, and Cdc42, as potential upstream regulators of membrane fusion. The RhoA downstream effector myosin II is required for fusion as the expression of mutant myosin light chain reduced membrane fusion. Furthermore, an inhibitor of the Arp2/3 complex, a downstream effector of Rac1 and Cdc42, also reduced self-contact-induced membrane fusion. At self-contacts, while the concentration of E-cadherin diminished, the intensity of GFP-tagged Arp3 rapidly fluctuated then decreased and stabilized after membrane fusion. Taken together, these data suggest that the Arp2/3 complex-mediated actin polymerization brings two opposing membranes into close apposition by possibly excluding E-cadherin from contact sites, thus promoting membrane fusion at self-contacts.

Plasma membrane fusion is a highly regulated process requiring multiple steps; the initial recognition by cell-cell adhesion molecules, close apposition of two opposing membranes, and finally, phospholipid mixing that leads to membrane fusion. In addition to cell-to-cell or vesicle fusion, plasma membranes of a single cell also fuse. In *Caenorhabditis elegans*, a fusion process, termed auto-fusion, fuses two opposing plasma membrane regions of a single cell to remove self-contacts (1–3). Furthermore, during neuronal development in *C. elegans*, overlapping neurites undergo auto-fusion to maintain proper dendritic branching, a process mediated by the fusogen EFF-1 (1). In mammalian epithelial and endothelial cells, self-junctions are removed through self-contact-induced membrane fusion (4). Interestingly, membrane fusion of endothelial cells is a key step in the formation of seamless capillaries (5, 6).

Fusogens, or fusogenic machinery, are required for cell fusion. In *C. elegans*, the fusogens EFF-1 and AFF-1 drive membrane fusion in cell-cell and auto-fusion (7). In mammalian cell fusion, only syncytins have thus far been identified as *bona fide* fusogens and are responsible for trophoblast fusion in the placenta (8). However, syncytin-1 may also be involved in cancer cell fusion (9), osteoclast fusion (10), and fertilization (11). Once membranes are brought into contact with fusogens, a mixing of the two membrane bilayers forms a hemifusion intermediate, and fusion may then proceed (12). Although some progress has been made in understanding cell-to-cell fusion, the molecular components and regulation of self-contact-induced membrane fusion remain unclear.

Although actin polymerization is required for cell adhesion and cell migration, very little is known about actin dynamics at self-contact-induced membrane fusion. Using dominant negative constructs and specific inhibitors, we tested Rho GTPases, upstream regulators of actin organization dynamics, during membrane fusion. Furthermore, we analyzed myosin II, a downstream effector of RhoA, and the Arp2/3[2] complex, a downstream effector of Rac1 and Cdc42 activation, in membrane fusion. Our results demonstrate a unique role of the Arp2/3 complex-induced actin assembly in the organization of E-cadherin at self-contacts.

EXPERIMENTAL PROCEDURES

Cell Lines and Reagents—Madin-Darby canine kidney (MDCK) GII cells were cultured in Dulbecco's modified Eagle's medium (low glucose) supplemented with 10% (v/v) fetal bovine serum, penicillin, streptomycin, and kanamycin. NSC23766, (−)-blebbistatin, phalloidin, CK-689, and CK-666

* This work was supported, in whole or in part, by National Institutes of Health Grant EUREKA GM094798 (to S. Y.).
[S] This article contains supplemental Movies 1–7.
[1] To whom correspondence should be addressed: Dept. of Biomedical Engineering, University of California, Davis, 451 Health Sciences Dr., GBSF 2317, Davis, CA. Tel.: 530-754-7251; Fax: 530-754-5739; E-mail: syamada@ucdavis.edu.

[2] The abbreviations used are: Arp, actin-related protein; MDCK, Madin-Darby canine kidney; ROCK, Rho-associated protein kinase; DN, dominant-negative; MLC, myosin regulatory light chain; ANOVA, analysis of variance.

were from Calbiochem. ML 141 was from Tocris (Bristol, UK). Monoclonal IgGs against Arp3 was from BD Biosciences, and polyclonal IgGs against non-muscle myosin IIA were from Sigma. Addgene (Cambridge, MA) plasmids 12599 (pcDNA3-EGFP-Cdc42), 12601 (pcDNA3-EGFP-Cdc42-T17N), 13719 (pcDNA3-EGFP-Rac1), and 13721 (pcDNA3-EGFP-Rac1-T17N) as well as RhoA wild-type and mutant T19N plasmids, were generated by Klaus Hahn (University of North Carolina). Cells were transfected using Lipofectamine 2000 (Invitrogen). MDCK cells stably expressing Arp3-GFP (13), myosin IIA-specific shRNA (14), myosin regulatory light chain (MLC)-GFP wild-type, and MLC-GFP TASA mutant were maintained with 100 μg/ml G418. Stable Arp3-GFP cells were transiently transfected with tandem dimer DsRed tagged E-cadherin for dual co-localization analysis.

Microfabrication of Pillar Array—The polydimethylsiloxane micropillar array was fabricated as previously described using standard soft lithography technique (4). The dimensions of individual pillars were 20 μm in height and 5 μm in diameter and arranged in a series of hexagons with an 18-μm pitch along each hexagon side. To view pillar dimensions, pillars were stained with CellTracker CM-DiI (0.5 μg/ml, Molecular Probes, Eugene, OR). All pillar substrates were coated with rat tail collagen type I (50 μg/ml, BD Biosciences). Cells were either seeded at confluence and incubated for up to 6 h or grown to confluence over the course of 24–48 h on the pillar array. Cells were fixed with 3% (v/v) paraformaldehyde containing 0.3% (v/v) Triton X-100 for 10 min and then stained with AlexaFluor 488/568-phalloidin (Invitrogen).

Microscopy—Cells were imaged using a Zeiss AxioObserver equipped with a Yokogawa CSU-10 spinning disk confocal system, 40× or 10× objectives, 488- and 561-nm solid-state lasers, and a Photometrics CoolSNAP HQ camera. The microscope system was controlled by Slidebook software (Intelligent Imaging Innovations, Denver, CO). For live-cell imaging, the temperature was set to 37 °C by a custom microscope heating chamber.

For scanning electron microscopy, cells were seeded onto collagen-coated pillar substrates that were micro-fabricated on 12-mm diameter round coverslips. Cells were quickly washed twice with 50% (v/v) 0.2 M Sorensen's phosphate buffer (Electron Microscopy Sciences, Hatfield, PA), fixed with Karnovsky's fixative for 15 min, then washed 3 times with 50% (v/v) 0.2 M Sorensen's phosphate buffer. Samples were then incubated with ethanol (Electron Microscopy Sciences), then hexamethyldisilazane (Ted Pella Inc., Redding, CA), and dried at room temperature. All samples were gold sputter-coated and viewed with a scanning electron microscope.

Quantification of Self-contact-induced Membrane Fusion—The method to quantify self-contact-induced membrane fusion has been described previously (4). Briefly, cells on self-contact-inducing substrates were trypsinized to remove cell adhesion sites including self-junctions, then stained with phalloidin. Fused cells remained with the pillars without obvious self-junctions. Results comparing two groups were analyzed using a two-tailed, unpaired Student's *t* test. Results comparing a single factor between three groups were analyzed using one-way ANOVA; significance was determined using Dunnett's post hoc test. Results were considered significant with $p < 0.05$.

Quantification of Fluorescence Intensity—To quantify fluorescence intensities surrounding individual pillars, we defined an annular region of interest bounded by the pillar (inner) circumference and concentric outer circle with the radius enlarged by 0.6 μm of the pillar radius. For self and cell-cell contacts, a freehand region of interest of the self-contact or along one representative side of each cell (cell-cell contact) was defined to measure fluorescence intensities and adjusted as contacts moved. Mean intensities within the region of interest surrounding the pillars and along cell contacts were measured every minute and then normalized with the basal fluorescence of the cell of interest (average intensity of five separate regions of interest within the cell) to correct for expression levels in different cells. All time-lapse images were first registered based on differential interference contrast images using ImageJ.

To characterize the dynamics of the Arp2/3 complex, we analyzed the accumulation of Arp3 by quantifying the overall GFP intensities and the fluctuations in Arp3 signal by quantifying the deviation of GFP signals. Overall fluorescence intensities were calculated as average intensities over the course of the time lapse. Fluorescence intensity deviations were calculated from the rolling intensity values (with $\pm$ 5 min windows) by taking the square root of the squared difference between the rolling average and actual intensities for each time point.

To compare the Arp3 dynamics at pre- and post-membrane fusion, we identified self-contacts via confocal microscopy. Before and after each time-lapse, z-stack images were taken to determine if pillars were surrounded by continuous cells (fused) or discontinuous cells (self-contacts). Pillars were subsequently categorized as post-fusion (continuous cells before and after time-lapse), pre-fusion (discontinuous cells before and after time-lapse), or fusing (discontinuous cells before and continuous after time-lapse). Of the 45 pillars analyzed, 14 were categorized as post-fusion, 13 as pre-fusion, and 9 as fusing. Nine pillars were not categorized due to cell division (6), or the status of the cells surrounding the pillars was not discernible (3).

Data points were considered outliers if mean intensities were >1.5× interquartile range below the first quartile or above the third quartile. For example, the normalized intensity surrounding one of the pillars in pre-fusion conditions was greater than the rest of the pre-fusion population, found to be an outlier and not included in further statistical analyses (see the *dot plot* in Fig. 3*F*). Results comparing a single factor between three groups were analyzed using one-way ANOVA, and significance was determined using Bonferroni's all pairs comparison or Dunnett's post-hoc test compared with a single control. Results were considered significant with $p < 0.05$.

RESULTS

A Micro-fabricated Pillar Array Promotes Self-contact-induced Membrane Fusion—To promote the formation of cell self-contacts, MDCK epithelial cells were plated on a micro-fabricated pillar array with individual pillars measuring 20 μm high and 5 μm in diameter and arranged in a series of hexagons with an 18-μm pitch along each hexagon side (Fig. 1*A*) (4). The

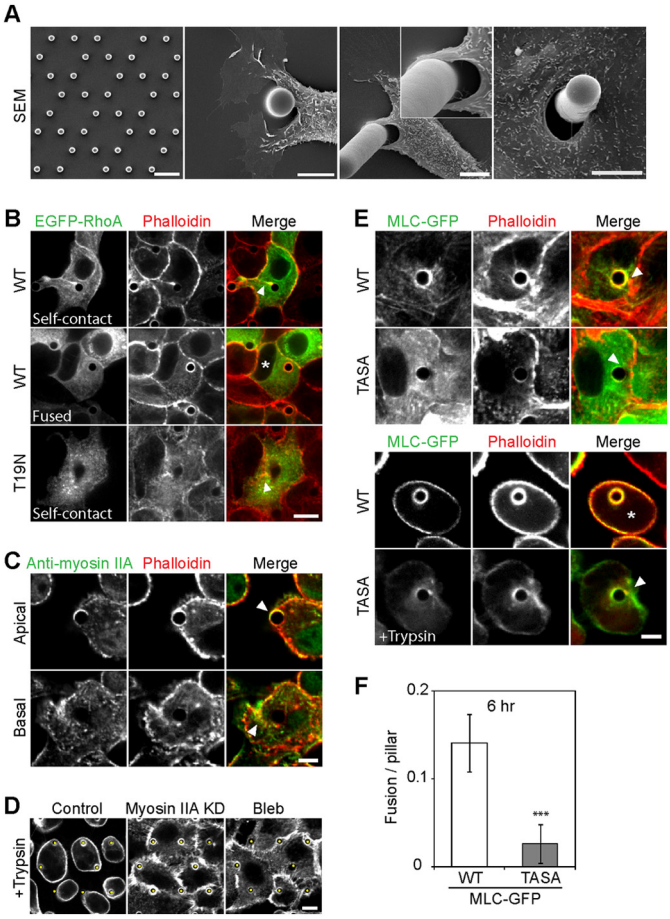

FIGURE 1. **Self-contact induced membrane fusion depends on myosin activity.** *A*, scanning electron micrographs (*SEM*) of a micro-fabricated pillar array designed to promote cell self-contact formation. Both single cells and cells within a colony wrap around individual pillars and ultimately fuse to become continuous around the pillar. *Scale bars* 20 (*left panel*) and 5 μm (*remaining panels*). *B*, WT and dominant-negative (*T19N*) GFP-tagged RhoA (*EGFP-RhoA*) both accumulated at self-contacts (*arrowheads*), but only WT RhoA-expressing cells were fused (*asterisk*). *Scale bar*, 10 μm. *C*, MDCK cells were seeded onto pillar substrates for 2 h, fixed, and probed with an anti-myosin IIA antibody and phalloidin-stained. Myosin IIA co-localizes with actin along the self-contact at both basal and apical layers (*arrowhead*, 7 μm between z-sections). *Scale bar*, 10 μm. *D*, MDCK cells were seeded onto the pillar substrate, trypsin-treated, fixed, and phalloidin-stained. Trypsin separated cell-cell contacts in WT cells (*Control*) but not in myosin IIA shRNA-expressing cells (myosin IIA KD), and WT cells treated with 10 μM blebbistatin (*Bleb*) and fusion could not be compared quantitatively. *Scale bar*, 5 μm. *E*, MDCK cells expressing MLC-GFP WT or MLC-GFP TASA mutant were seeded onto the pillar substrate for 6 h, fixed, and phalloidin-stained. *Top panels*, both WT and mutant cells formed self-contacts around pillars (*arrowheads*). *Bottom panels*, cells were treated with trypsin before fixation. MLC-GFP WT expressing cells fused (*asterisk*), whereas mutant cells did not. *Scale bar*, 5 μm. *F*, quantitative analysis of membrane fusion from MLC WT and MLC TASA mutant expressing cells displayed as mean fusion/pillar $\pm$ S.D. Statistics analyzed with Student's *t* test assuming equal variance (number of pillars analyzed: WT (347), TASA (308); ***, $p < 0.001$].

design of the pillar array allowed opposing membrane extensions from single cells to spread around individual pillars to form self-contacts (Fig. 1*A*). The cells, whether as single cells or cells within a monolayer, remain wrapped around the pillars (Fig. 1*A*) even after trypsin digest to remove cell junctions, suggesting that self-contacts were eliminated by membrane fusion (4). This unique system provides an experimental platform to tease out the parameters required for this membrane fusion.

The Activity of the Small GTPase RhoA Affects Membrane Fusion at Self-contacts—The Rho GTPase family members play critical roles in regulating actin dynamics and cell-cell fusion. Thus, we examined the contribution of three main members of the Rho GTPase family (RhoA, Rac1, and Cdc42) to self-contact-induced membrane fusion. To test RhoA, Rac1, and Cdc42 in self-contact-induced membrane fusion, we transiently expressed dominant-negative (DN) mutants with a GFP tag in MDCK cells.

Both wild-type (WT)-RhoA- and DN-RhoA-expressing cells formed self-contacts. While the RhoA constructs localized to self-contacts, only WT-RhoA expressing cells fused around the pillars (Fig. 1*B*). We previously showed that ROCK inhibitors reduce self-contact-induced membrane fusion, presumably by reducing myosin II activity (4). The absence of membrane fusion at self-contacts in DN-RhoA-expressing cells suggests that RhoA is likely an upstream regulator of ROCK and myosin II, and cell contractility through the Rho/ROCK pathway is a key process mediating self-contact-induced membrane fusion.

To test the roles of myosin II in self-contact-induced membrane fusion, we analyzed the localization of myosin II at self-contacts. The antibody-labeled myosin IIA, a predominant myosin II isoform in MDCK cells (14), localized around the pillar as well as along self-contacts (Fig. 1*C*). To analyze the efficiency of membrane fusion around the pillars, cells were briefly digested with trypsin to remove self- and cell-cell contacts, thus leaving behind only fused cells around the pillars (Fig. 1*D*, *Control*). Using myosin IIA-deficient cells (14) or cells treated with blebbistatin, a myosin II-specific inhibitor, trypsin digest could not separate adhesive contacts (Fig. 1*D*), thus making discrimination between fused cells from self-contacting cells difficult. As an alternate approach, myosin regulatory light chain (MLC) with alanine substitutions at phosphorylation sites was transfected into MDCK cells and compared with WT MLC expressing MDCK cells (Fig. 1*E*). The GFP-tagged MLC localized around the pillars and at self-contacts (Fig. 1*E*). Unlike myosin IIA-deficient cells or blebbistatin-treated cells, the MLC mutant-expressing cells still retracted upon trypsin digest to enable the fusion quantification. Yet, trypsin digest revealed significantly reduced membrane fusion around the pillars in the mutant-expressing cells (Fig. 1*F*), suggesting that membrane fusion is highly sensitive to myosin II activity and upstream signaling from RhoA.

The Activity of Rac1 and Cdc42 Affect Membrane Fusion at Self-contacts—Both WT-Rac1- and DN-Rac1-expressing cells formed self-contacts with a strong accumulation of both Rac1 and actin filaments at self-contacts and around the pillars. Although we observed WT-Rac1-expressing cells fused around individual pillars, we did not observe pillar-bound-fused membranes in DN-Rac1-expressing cells (Fig. 2*A*). Similar to Rac1, both WT-Cdc42- and DN-Cdc42-expressing cells formed self-contacts and accumulated at self-contacts and around pillars, but unlike Rac1, membrane extensions of WT and some DN-Cdc42-expressing cells fused around pillars (Fig. 2*B*).

Because Rac1 and Cdc42 have distinct downstream effectors from the RhoA signaling pathway, these downstream molecules may reveal new mechanistic details on self-contact-induced membrane fusion. Therefore, we further perturbed these Rho

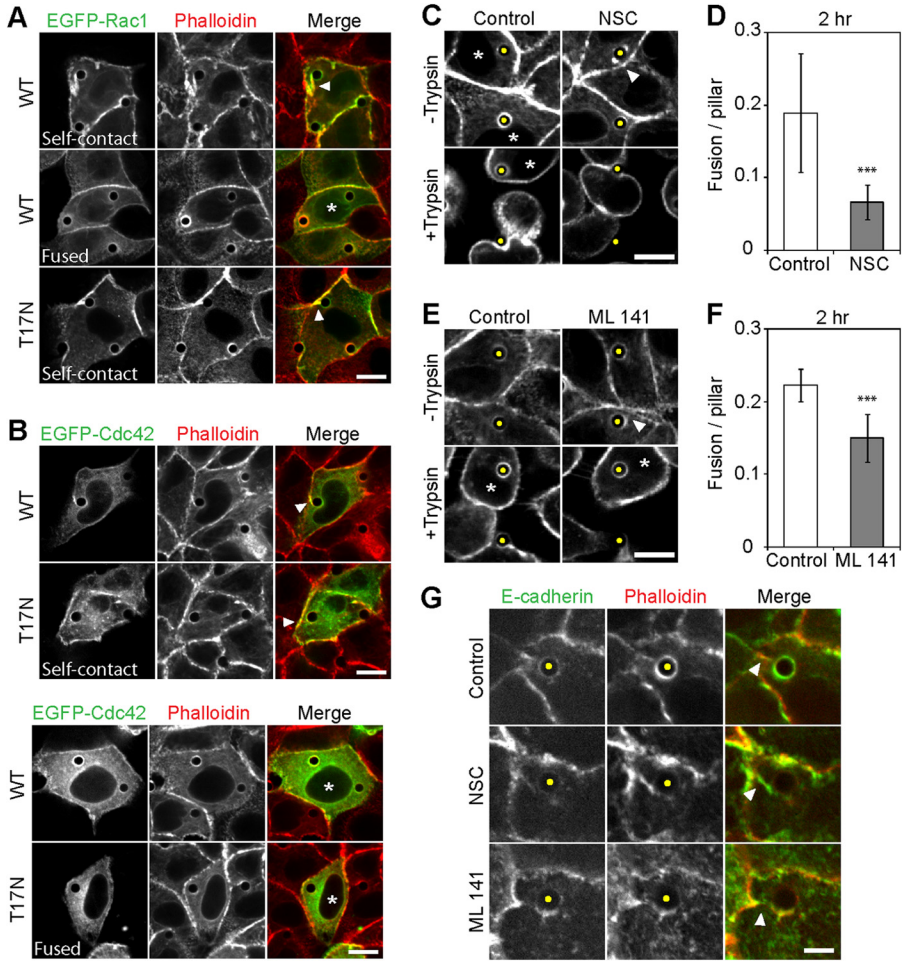

FIGURE 2. **Both Rac1and Cdc42 inhibition affect self-contact-induced membrane fusion.** *A*, WT and dominant-negative (*T17N*) GFP-tagged Rac1 (*EGFP-Rac1*) both accumulated at sites of self-contact, yet only WT Rac1-expressing cells were fused. *B*, WT and T17N GFP-tagged Cdc42 (*EGFP-Cdc42*) both accumulated at self-contacts. WT and some T17N Cdc42-expressing cells fused. *C*, MDCK cells were seeded at confluence on pillar substrates in the absence of serum for 1 h, then switched to normal serum containing media (*Control*) or one supplemented with 100 μM NSC23766 (*NSC*) for 2 h. The samples were either treated with trypsin or not, then phalloidin-stained. Control cells were fused around pillars, whereas NSC-treated cells were not (see + *Trypsin*). *D*, quantitative analysis of membrane fusion from control and NSC treatment groups displayed as the mean fusion/pillar ± S.D. Statistics were analyzed with Student's *t* test assuming unequal variance (number of pillars analyzed: control (391), NSC (389); ***, $p < 0.001$). *E*, MDCK cells seeded at confluence on pillar substrates in the absence of serum for 1 h and then switched to normal serum containing media (control) or one supplemented with 25 μM ML 141 for 2 h. The samples were either treated with trypsin or not, then phalloidin-stained. *Arrowheads* indicate self-contacts, and *asterisks* indicate fused cells. *Scale bars*, 10 μm (*A–C* and *E*). *F*, quantitative analysis of membrane fusion from control and ML 141 treatment groups displayed as mean fusion/pillar ± S.D. Statistics were analyzed with Student's *t* test assuming equal variance (number of pillars analyzed: control (319), ML 141 (319); ***, $p < 0.001$). *G*, MDCK cells expressing tandem dimer DsRed-tagged E-cadherin were seeded at confluence on pillar substrates in the absence of serum for 1 h, then switched to normal serum containing media (*Control*) or one supplemented with either 100 μM NSC or 25 μM ML 141 for 2 h, then fixed and phalloidin-stained. Self-contact formations (*arrowheads*) with E-cadherin and actin accumulation were present with inhibitor treatments. *Scale bar*, 5 μm. *Yellow dots* indicate pillar locations.

GTPases by specific small molecule inhibitors and analyzed the efficiency of self-contact-induced membrane fusion. MDCK cells were treated with either a Rac1-specific (NSC23766) or Cdc42-specific (ML 141) inhibitor. Due to Rac1 and Cdc42, both regulating cell spreading and motility, these inhibitors will also reduce the chance of two extending membranes from single cells to wrap around the pillars to form self-contacts. To circumvent this issue, cells were initially seeded at confluence in the absence of serum, which suppresses membrane fusion at self-contacts, while cells still adhere and spread around individual pillars to establish self-contacts (4). A subsequent introduction of serum with inhibitors could then selectively test the ability of self-contacts to fuse instead of affecting the self-contact formation.

Using trypsin treatment to separate cell-cell and self-contacts to identify fused cells around pillars (Fig. 2, *C* and *E*), both NSC23766 and ML 141 significantly decreased membrane fusion at self-contacts compared with respective control conditions, albeit the reduction of fusion was greater in the presence of the NSC23766 inhibitor (Fig. 2, *D* and *F*). To tease out defects in fusion due to either cell adhesion or membrane fusion, we tested whether inhibitor-treated cells are capable of maintaining self-contacts by analyzing E-cadherin localization. In the presence of NSC23766 or ML 141 inhibitor, E-cadherin localized to self-contacts, suggesting that cells were still capable of maintaining self-junctions despite NSC23766 or ML 141 treatment (Fig. 2*G*). Therefore, the reduction of fused membrane around the pillars was not due to the failure of cells to maintain self-contacts around individual pillars but, rather, to intrinsic defects during membrane fusion. Although some DN-Cdc42-expressing cells appeared to be fused around the pillars (Fig. 2*B*), the quantitative analysis using the inhibitors

demonstrated that both Rac1 and Cdc42 suppress the fusion activity at self-contacts.

High Arp2/3 Dynamics Promote Self-contact-induced Membrane Fusion—To identify the Rac1 and Cdc42 downstream effectors that promote membrane fusion, we focused on the Arp2/3 complex, a potent actin nucleator that promotes the growth of actin network at the leading edge of migrating cells. In fixed cells, GFP-tagged Arp3, a component of the Arp2/3 complex, co-localized with phalloidin-labeled actin at sites of self-contact at a level similar to cell-cell contacts (Fig. 3*A*). In live-cell confocal imaging, Arp3-GFP formed puncta, and its intensity was discontinuous along cell-cell and self-contacts, thus making precise localization at self-contacts difficult. We define the pre-fusion state by scanning z-sections and finding Arp3-GFP localization that resembles self-contacts. In the absence of such localization, the membranes were defined as post-fusion. Arp3-GFP rapidly and transiently accumulated at self-contacts and subsequently dissipated as cells fused around individual pillars (Fig. 3*B*, supplemental Movie 1). Interestingly, Arp3-GFP also localized around the pillars adjacent to self-contacts with its intensity, often exceeding that of self and cell-cell contacts, rapidly fluctuating (Fig. 3, *B* and *C*). To determine the extent of the intensity fluctuations, we calculated intensity deviations (see "Experimental Procedures") over time (Fig. 3*C*). As cells transitioned from self-contact to fused, the fluctuating Arp3-GFP intensities surrounding the pillars dimmed and stabilized (Fig. 3*C*, see another example in Fig. 3*D*, supplemental Movie 2).

To further investigate the relationship between Arp3 surrounding the pillars and the state of the self-junctions (*i.e. pre-versus* post-fusion), we monitored Arp3-GFP intensity in confluent cells on the pillar substrate over the course of 3 h. The fluorescence intensities in post-fusion membranes remained dim and stable (Fig. 3*E*, supplemental Movie 3), whereas intensities in pre-fusion membranes were highly variable (Fig. 3*E*, supplemental Movie 4). The mean intensities of pre-fusion contact surrounding the pillars were greater than in post-fusion pillars (Fig. 3*F*). Additionally, intensities surrounding the pillars fluctuated throughout the time-lapse in pre-fusion membranes compared with the relatively stable intensities displayed in post-fusion membranes (Fig. 3*G*). Interestingly, the pre-fusion mean intensities and deviations surrounding the pillars were greater than at cell-cell contacts (Fig. 3, *F* and *G*), suggesting distinct Arp2/3 complex dynamics at self-contacts *versus* normal cell-cell contacts.

Arp2/3 Activity Is Required for Self-contact-induced Membrane Fusion—We hypothesized that this Arp2/3 dynamics may be required for membrane fusion and tested the requirement of Arp2/3 activity in self-contact-induced membrane fusion using the Arp2/3-specific inhibitor CK-666. In immunostained wild-type cells, CK-666 decreased Arp3 at sites of self- and cell-cell contact as well as surrounding the pillars despite the presence of phalloidin labeled actin (Fig. 4*A*). In live-cell imaging, CK-666 decreased Arp3-GFP accumulation surrounding the pillars and at cell-cell contacts (Fig. 4*B*), suggesting the Arp2/3 complex is quickly inactivated in the presence of CK-666. Furthermore, in the presence of CK-666, self and cell-cell junctions remained intact with positive E-cadherin localization (Fig. 4*B*), albeit with a slight reduction in E-cadherin intensity. To analyze the effect of inhibitors on the accumulation and fluctuation of the Arp2/3 complex, we quantified Arp3-GFP intensity and deviation surrounding the pillars after drug treatment. Compared with CK-689 control, both Arp3-GFP intensity and deviation significantly decreased in the presence of CK-666 (Fig. 4*C*). In contrast, inhibition of the upstream regulators of the Arp2/3 complex, Rac1 and Cdc42, had less impact on both Arp3-GFP intensity and deviation (Fig. 4*C*).

The effects of CK-666 on self-contact-induced membrane fusion were tested using the same inhibitor protocol for Rac1 and Cdc42 inhibitors. Although CK-666-treated cells were capable of forming self-contacts (Fig. 4*D*, *−Trypsin*, *arrowheads*), fusion decreased in a dose-dependent manner in comparison to the inactive CK-689 control (Fig. 4*E*). These data point to a direct role of the Arp2/3 complex in self-contact-induced membrane fusion.

High Arp2/3 Activity Is Concurrent with Loss of E-cadherin at Self-contacts—The Arp2/3 complex is required for lamellipodia extension that promotes the formation of new focal adhesions during cell migration. Therefore, we sought whether the Arp2/3 complexes promote the engagement or clustering of E-cadherin at self-junctions. We expressed tandem dimer DsRed-tagged E-cadherin and GFP-tagged Arp3 in MDCK cells. In live-cell imaging, E-cadherin was strongly concentrated at self-contact (Fig. 5*A*, *arrowhead*; supplemental Movie 5), whereas Arp3-GFP accumulated surrounding the pillar (Fig. 5*A*, supplemental Movie 6). As E-cadherin localization at self-contact became discontinuous, both E-cadherin and Arp3 intensities diminished (Fig. 5*A*, supplemental Movie 7). Upon closer examination, E-cadherin intensity initially became discontinuous immediately adjacent to the pillar (Fig. 5*B*, 14 min, *arrow*), where the Arp3 intensity was the highest at the side of the pillar facing the self-contact (Fig. 5*B*, 14 min). As E-cadherin intensity dissipated along the self-contact adjacent to the pillar (Fig. 5, *B* and *C*, 14 min), the Arp3 intensity remained high, albeit the Arp3 intensity slowly diminished after the E-cadherin intensity became discontinuous along the self-contact (Fig. 5*C*, 14 min and beyond). The reason for this gradual response of the Arp2/3 activity to membrane fusion is not clear, however. Eventually, both E-cadherin and Arp3 decreased to basal expression levels (Fig. 5*C*, 60 min). Unlike the canonical function of the Arp2/3 complex that promotes adhesion, these results suggest that high Arp2/3 activity promotes membrane fusion while E-cadherin dissipates from self-contacts.

DISCUSSION

The fusion of membranes is a multistep process (membrane adhesion, close apposition of the membranes, and fusion) requiring careful, multifaceted regulation. All three small GTPases analyzed, RhoA, Rac1, and Cdc42, compromise the efficiency of self-contact-induced membrane fusion, albeit at different degrees. The expression of DN-RhoA decreases the observed membrane fusion around the pillars (Fig. 1*B*). This is consistent with previous observations that ROCK inhibition and ROCK1/2 knockdown also decrease the efficiency of self-contact-induced membrane fusion (4).

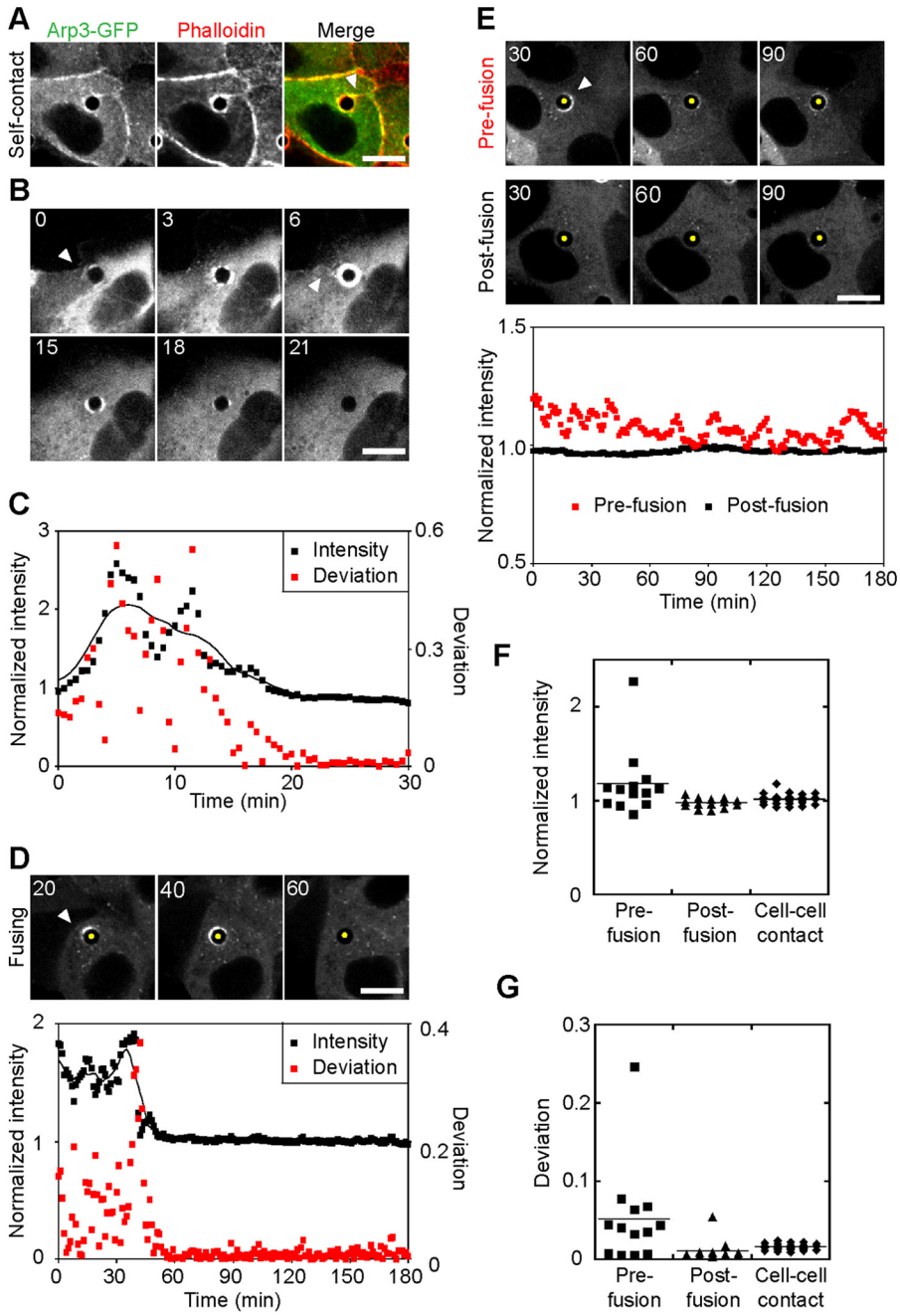

FIGURE 3. **The Arp3 localization and dynamics at the sites of cell self-contacts.** *A*, MDCK cells expressing GFP-tagged Arp3 grown for 24 h on the pillar array, fixed, and phalloidin-stained. The fluorescence signal from Arp3-GFP accumulates at self-contacts (*arrowhead*). *B*, time-lapse imaging of GFP-tagged Arp3 expressing MDCK cells forming self-contacts. Cells were seeded onto the pillar array 24 h before imaging. Based on the Arp3-GFP signal, the Arp2/3 complex accumulates at self-contacts (*arrowhead*) and around the individual pillars then dissipates over time. Time is in minutes. *C*, normalized Arp3-GFP intensity (*black squares*), rolling average intensity (*line*), and intensity deviation (*red squares*) surrounding a pillar (from Fig. 3*B*) over time. *D*, Arp3-GFP expressing MDCK cell fusing around a pillar. Arp3-GFP accumulates at the site of self-contact (*arrowhead*) and around the pillar and dissipates as the cell becomes fused. Time is in min. The graph displays normalized Arp3-GFP intensity (*black squares*) and intensity deviation (*red squares*) over time. Cells were grown for 24 h on the pillar array before live-cell imaging. *E*, time-lapse imaging of pre-fusion (*top*) and post-fusion (*bottom*) cells. The *arrowhead* points to the pre-fusion site. The graph displays normalized Arp3-GFP intensity over time of a pre-fusion cell (*red*) that has a fluctuating Arp3-GFP intensity surrounding the pillar and a post-fusion cell (*black*) that remains dim and relatively stable throughout the time-lapse. Time is in minutes. *F*, dot plot of normalized mean Arp3-GFP intensities surrounding pillars in post-fusion conditions ($n = 14$), pre-fusion ($n = 13$) conditions, and along cell-cell contacts ($n = 25$). Pre-fusion conditions had greater Arp3-GFP intensities surrounding pillars over post-fusion ($p < 0.01$) and cell-cell contacts ($p < 0.05$). *G*, dot plot of intensity deviations from post-fusion conditions, pre-fusion conditions, and along cell-cell contacts. Pre-fusion conditions had greater intensity deviations over post-fusion ($p < 0.001$) and cell-cell contacts ($p < 0.01$). Statistics analyzed with one-factor ANOVA followed by Bonferroni's all pairs comparison. *Yellow dots* indicate pillar locations. *All scale bars*, 10 μm.

A possible function of the Rho/ROCK pathway in membrane fusion is the activation of a down-stream effector, myosin II. In fact, the mutant form of myosin regulatory light chain significantly reduced membrane fusion (Fig. 1, *E* and *F*). In cell-to-cell fusion of mouse myoblasts, the activity of non-muscle myosin IIA promotes the formation of cortical actin bundles along the fusion sites of myoblasts, and myosin IIA inhibition prevents myoblast fusion (15). Interestingly, myosin II activation has

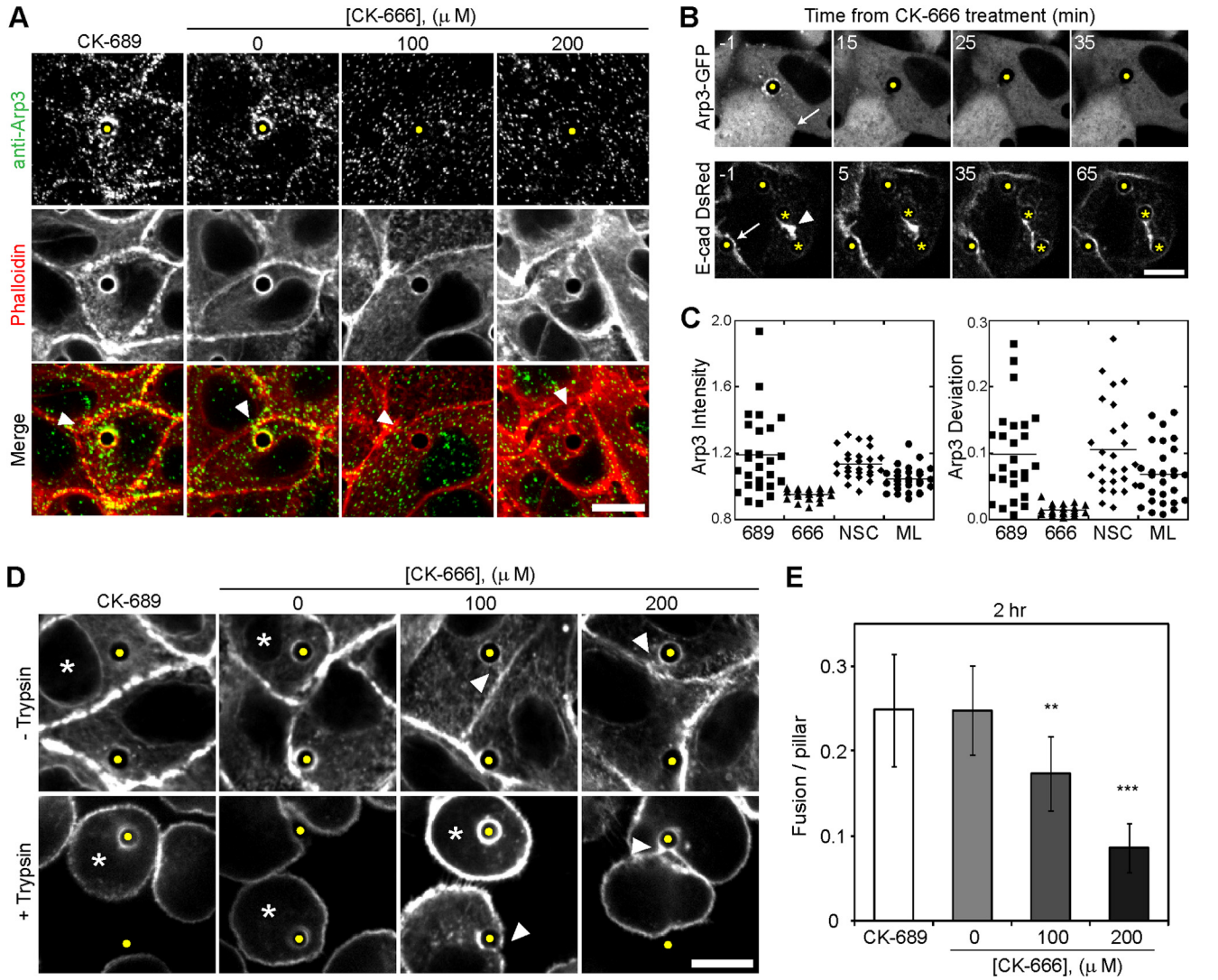

FIGURE 4. **Arp2/3 inhibitor reduces Arp3 accumulation and membrane fusion at self-contacts.** *A*, comparison of Arp3 localization at sites of self-contact (*arrowheads*) in MDCK wild-type cells treated with CK-689 or CK-666 (0, 100, and 200 μM) for 2 h. Cells were immunostained with antibodies specific for Arp3 and counter-stained with phalloidin. Images are maximum projections of four z-sections covering 2 μm. *B*, *top panels*, Arp3-GFP expressing cells before and after 200 μM CK-666 treatment. Arp3-GFP was removed surrounding the pillar and at cell-cell contacts (*arrow*) in the presence of CK-666. *Bottom panels*, tandem dimer DsRed-tagged E-cadherin expressing cells before and after 200 μM CK-666 treatment. Self-contacts (*arrowhead*) and cell-cell contacts (*arrow*) remain intact in the presence of CK-666. Self-contact was formed surrounding a pillar that looped back down onto the substrate surface (*yellow asterisks*). *Yellow dots* indicate neighboring pillar locations. Time is in minutes from CK-666 treatment. *C*, dot plots of normalized mean Arp3-GFP intensity and intensity deviation surrounding pillars in cells treated with 200 μM CK-689 control ($n = 26$), 200 μM CK-666 ($n = 20$), 100 μM NSC23766 ($n = 26$), and 25 μM ML 141 ($n = 28$). Arp3-GFP intensity decreased with CK-666 ($p < 0.001$) and ML 141 ($p < 0.01$), whereas intensity deviations decreased with CK-666 ($p < 0.001$). Statistics were analyzed with one-factor ANOVA followed by Dunnett's post-hoc test compared with CK-689 control. *D*, comparison of membrane fusion in MDCK wild-type cells treated with CK-689 or CK-666 (0, 100, and 200 μM) for 2 h. Cells were stained with phalloidin. *Arrowheads* indicate self-contacts, and *asterisks* indicate fused cells. *E*, quantitative analysis of membrane fusion from CK-689 control and CK-666 treatment groups (0, 100, and 200 μM) displayed as mean fusion/pillar $\pm$ S.D. Statistics analyzed with one-factor ANOVA followed by Dunnett's post-hoc test (number of pillars analyzed: CK-689 control (353), untreated (0 μM CK-666; 371), 100 μM CK-666 (377), 200 μM CK-666 (359); **, $p < 0.01$; ***, $p < 0.001$ compared with CK-689). *Yellow dots* indicate pillar locations. *All scale bars*, 10 μm.

been implicated in the expansion of fusion pores during exocytosis (16); thus, membrane tension regulated by myosin II activity may be required for efficient membrane fusion at self-contacts. Alternatively, constitutively active RhoA also decreases myoblast fusion by de-stabilizing M-cadherins at cell-junctions (17). Because ROCK activity is essential for the proper organization of cadherins in nascent cell-cell adhesion (18), RhoA-induced cell contractility and actin organization may be required for priming the membrane fusion sites by organizing adhesion proteins.

In contrast to RhoA, the activation of Rac1 or Cdc42 promotes actin polymerization through the Arp2/3 complex by activating nucleation promoting factors such as Scar/WASP (Wiskott-Aldrich syndrome protein) proteins (19). Rac1 is required for myoblast fusion in *Drosophila* (20, 21), whereas both Rac1 and Cdc42 are required for mouse myoblast fusion (22). Actin rearrangement during myoblast fusion depends on nucleation-promoting factors (23, 24) to assist the Arp2/3 complex branching of the actin network. To highlight the importance of actin dynamics during fusion, reconstitution of fusion in a non-fusing cell line, even with the expression of a fusogen, still required actin-driven membrane protrusions to engage the fusogens on opposing membranes (25). The suppression of self-contact-induced membrane fusion with the Rac1 inhibitor was

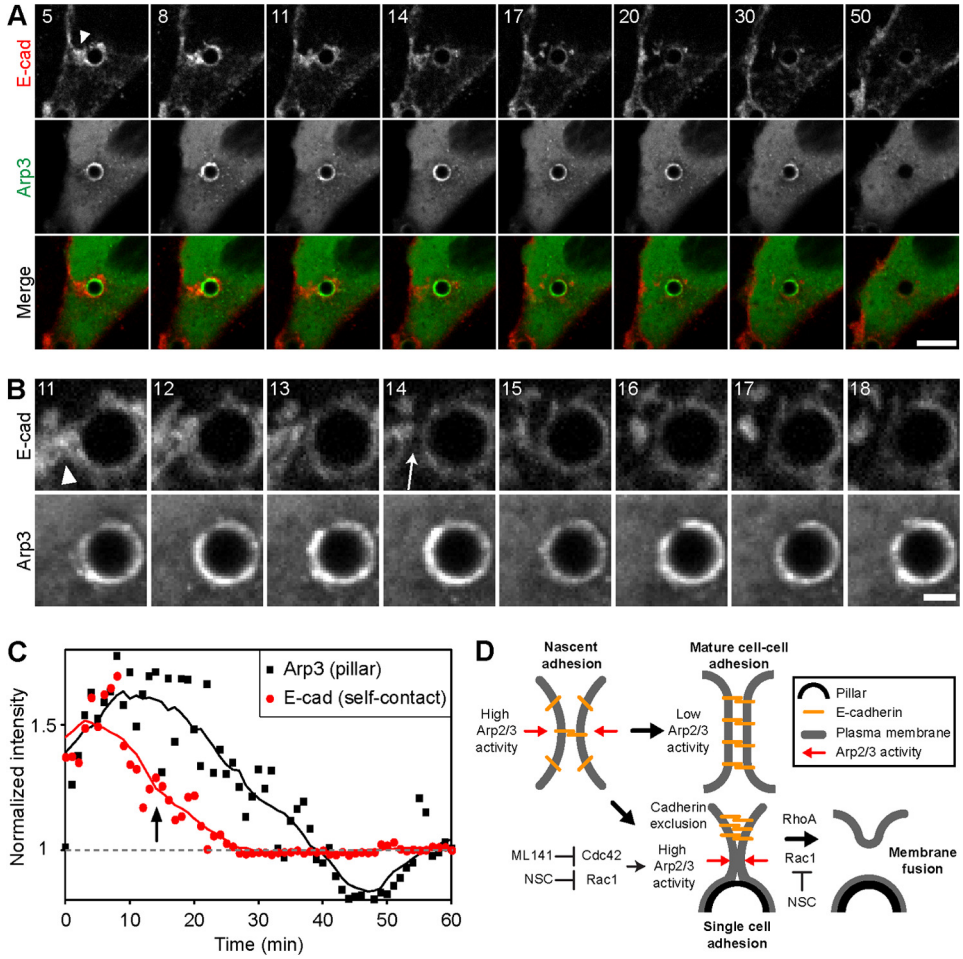

FIGURE 5. **The Arp2/3 and E-cadherin dynamics at cell self-contacts.** *A*, time-lapse images of Arp3 and E-cadherin at cell self-contact. Arp3-GFP-expressing cells were transfected with tandem dimer DsRed-tagged E-cadherin and seeded onto the pillar array 24 h before imaging. The *arrowhead* indicates self-contact. Time is in minutes. *Scale bar*, 10 μm. *B*, enlarged time-lapse images (from Fig. 5*A*) with strong E-cadherin accumulation at self-contact (min 11, *arrowhead*) and a subsequent loss of E-cadherin near the pillar (min 14, *arrow*) with a concurrent increase in Arp3. Time is in minutes. *Scale bar*, 2 μm. *C*, graph of normalized intensities of Arp3-GFP surrounding a pillar (*black squares*) and E-cadherin td-DsRed along self-contact (*red circles*) over time (from Fig. 5*A*). With a loss of E-cadherin along the self-contact near the pillar (Fig. 5*B*, min 14), Arp3 surrounding the pillar remains elevated (*arrow*). *D*, a model of self-contact-induced membrane fusion. Initial self and cell-cell adhesions are initiated by adhesion between E-cadherin and lamellipodia extensions with high Arp2/3 activity. Mature cell-cell adhesions have E-cadherin accumulation with decreased Arp2/3 activity, whereas self-adhesions have E-cadherin exclusion near the pillars and high Arp2/3 activity that is mediated by Cdc42. For fusion to proceed, both RhoA and Rac1 activity are required.

more robust than with the Cdc42 inhibitor (Fig. 2, *D* and *F*), suggesting that Rac1 activity plays a more substantial role than Cdc42 in self-contact-induced membrane fusion. Interestingly, however, the Cdc42 inhibitor suppressed the Arp3 dynamics at a greater extent than the Rac1 inhibitor, although maximum suppression of Arp3 dynamics was only observed with the Arp2/3 complex-specific inhibitor (Fig. 4*C*). It is likely that the role of Rac1 in self-contact-induced membrane fusion is not limited to the regulation of the Arp2/3 complex, but rather, Rac1 directs additional activities regulating membrane fusion, although the exact nature of this regulation remains unclear.

Membrane protrusions driven by actin polymerization have emerged as an essential process in membrane fusion. A key characteristic of self-contact-induced fusion is the accumulation of Arp3 surrounding the individual pillars before membrane fusion (Figs. 3–5). The dynamic nature of Arp3 around the pillars indicates rapid actin nucleation through the Arp2/3 complex during self-contact-induced membrane fusion. This is similar to how membrane protrusions generated by actin polymerization are required for fusogen engagement (24, 25). Whether finger-like membrane protrusions or pillar obstacles, these high curvature membrane structures may be selectively inducing actin polymerization until fusion is completed. Interestingly, in phagocytosis of oblong objects, internalization is prevented along the long axis, suggesting a preference toward high curvature regions as the sites of membrane fusion (26). In fact, surface curvature with a specific phospholipid composition has been shown to regulate actin dynamics (27), suggesting that membrane curvature may be a key parameter of actin polymerization and membrane fusion at nascent self-contacts. Similar to the formation of cell-cell adhesion that induces contact inhibition, this membrane activity is suppressed once fusion is completed.

How then does actin polymerization aid membrane fusion? Perhaps actin polymerization produces sufficient forces to bring two membranes into close apposition for lipid bilayer mixing. For example, the Arp2/3 complex-mediated actin polymerization can generate nanonewtons of forces sufficient

for many cellular movements (28). Actin assembly can also induce membrane scission of Shiga toxin-induced tubules, a process where mechanical force has been proposed as a potential mechanism (29). However, in clathrin-mediated endocytosis, actin assembly appears to be dispensable for membrane fission (30).

Interestingly, phagocytosis in macrophages provides a similar template to Arp2/3-mediated self-contact-induced membrane fusion. During phagocytosis, actin polymerization through the Arp2/3 complex promotes membrane extensions around particles from the initial cup formation to closure (31). Note, however, that close apposition of two membranes is not always sufficient for membrane fusion. In SNARE-mediated vesicle fusion, the lipid anchored (not transmembrane anchored) SNARE proteins, although able to form a tight SNARE complex, do not promote fusion (32) except in the presence of accessory proteins (33), suggesting that close apposition of membranes are not sufficient for SNARE-induced membrane fusion. Rather than the tight helical formation of the trans-SNARE complex that brings two opposing membranes together, the Arp2/3 complex-mediated actin assembly pushes two opposing membranes together and, thus, possibly by-passing the requirement for SNARE-like proteins.

One key obstacle to bringing two membranes in close apposition is the presence of transmembrane proteins. Engagement of E-cadherins initiates the formation of self-contacts (4) but also has a predicted intercellular spacing of ~37 nm (34), a distance too great for membrane fusion. In the case of the *C. elegans* fusion protein EFF-1, this intercellular spacing must be reduced to roughly 20 nm for the extracellular domain of EFF-1 to engage and membrane fusion to proceed (35, 36). Thus, E-cadherin must be cleared before fusion initiates. Indeed, E-cadherin concentration decreases at self-contact immediately adjacent to the pillar with a concurrent increase in Arp3 (Fig. 5). This E-cadherin movement may be due to exclusion from self-contacts by Arp2/3 complex-mediated actin polymerization before membrane fusion. Although it remains possible that E-cadherin exclusion is due to fusion pore expansion that pushes E-cadherin away from the fusion site. The limited resolution of the current method does not resolve the precise timing of membrane fusion to tease out the sequence of E-cadherin movement leading up to and after membrane fusion.

Interestingly, a high cytoplasmic α-catenin concentration at E-cadherin-mediated cell contacts prevents Arp2/3-mediated actin polymerization (37, 38) by competing for the surface of actin filaments with the Arp2/3 complex (39). The high Arp2/3 complex activity may overcome this inhibition by excluding E-cadherin from self-contacts and suppressing local α-catenin concentration (see the model in Fig. 5). The exclusion of E-cadherin and α-catenin at self-contacts could be a discriminatory factor that determines contact maturation *versus* fusion of membrane contacts (Fig. 5).

Despite similar surface chemistries, strong Arp3 localization and dynamics at self-contacts (and surrounding the pillars) *versus* cell-cell contacts (Fig. 3, *F* and *G*) highlights functionally distinct outcomes between these two types of contacts. Cell-cell contacts between epithelial cells mature, whereas self-contacts can undergo membrane fusion, suggesting that normal epithelial cells distinguish between binding self *versus* neighboring cells. Fusion as a self-recognition process has been observed during neuronal development in *C. elegans* where overlapping neurites can undergo auto-fusion to maintain proper dendritic branching, a process mediated by the fusogen EFF-1 (1). Although we do not know the fusogen responsible for self-contact-induced membrane fusion, we demonstrate that the efficient self-contact-induced membrane fusion observed in mammalian epithelial cells is regulated by Rho GTPases and their downstream effectors, the Arp2/3 complex and myosin II. The mechanism of self-contact-induced membrane fusion may have further implications in similar membrane self-contacting events with membrane closure during phagocytosis as well as in cell-to-cell fusion.

Acknowledgments—We thank Drs. Matt Welch (University of California, Berkeley), Klaus Hahn (University of North Carolina), and Michael Olson (Beatson Institute for Cancer Research) for the Arp3-GFP plasmid, small GTPase plasmids, and MLC-GFP plasmids, respectively. We thank Dr. Wenting Shih for generating the Myosin IIA shRNA, MLC-GFP wild-type, and TASA mutant stably expressing cell lines. Also, we thank Mary Sedarous for helping with E-cadherin stability experiments.

REFERENCES

1. Oren-Suissa, M., Hall, D. H., Treinin, M., Shemer, G., and Podbilewicz, B. (2010) The fusogen EFF-1 controls sculpting of mechanosensory dendrites. *Science* **328,** 1285–1288
2. Rasmussen, J. P., English, K., Tenlen, J. R., and Priess, J. R. (2008) Notch signaling and morphogenesis of single-cell tubes in the *C. elegans* digestive tract. *Dev. Cell* **14,** 559–569
3. Stone, C. E., Hall, D. H., and Sundaram, M. V. (2009) Lipocalin signaling controls unicellular tube development in the *Caenorhabditis elegans* excretory system. *Dev. Biol.* **329,** 201–211
4. Sumida, G. M., and Yamada, S. (2013) Self-contact elimination by membrane fusion. *Proc. Natl. Acad. Sci. U.S.A.* **110,** 18958–18963
5. Lammert, E., and Axnick, J. (2012) Vascular lumen formation. *Cold Spring Harb. Perspect. Med.* **2,** a006619
6. Lenard, A., Ellertsdottir, E., Herwig, L., Krudewig, A., Sauteur, L., Belting, H. G., and Affolter, M. (2013) *In vivo* analysis reveals a highly stereotypic morphogenetic pathway of vascular anastomosis. *Dev. Cell* **25,** 492–506
7. Aguilar, P. S., Baylies, M. K., Fleissner, A., Helming, L., Inoue, N., Podbilewicz, B., Wang, H., and Wong, M. (2013) Genetic basis of cell-cell fusion mechanisms. *Trends Genet.* **29,** 427–437
8. Mi, S., Lee, X., Li, X., Veldman, G. M., Finnerty, H., Racie, L., LaVallie, E., Tang, X. Y., Edouard, P., Howes, S., Keith, J. C., Jr., and McCoy, J. M. (2000) Syncytin is a captive retroviral envelope protein involved in human placental morphogenesis. *Nature* **403,** 785–789
9. Bjerregaard, B., Holck, S., Christensen, I. J., and Larsson, L. I. (2006) Syncytin is involved in breast cancer-endothelial cell fusions. *Cell. Mol. Life Sci.* **63,** 1906–1911
10. Søe, K., Andersen, T. L., Hobolt-Pedersen, A. S., Bjerregaard, B., Larsson, L. I., and Delaissé, J. M. (2011) Involvement of human endogenous retroviral syncytin-1 in human osteoclast fusion. *Bone* **48,** 837–846
11. Bjerregaard, B., Lemmen, J. G., Petersen, M. R., Østrup, E., Iversen, L. H., Almstrup, K., Larsson, L. I., and Ziebe, S. (2014) Syncytin-1 and its receptor is present in human gametes. *J. Assist. Reprod. Genet.* **31,** 533–539
12. Podbilewicz, B. (2014) Virus and cell fusion mechanisms. *Annu. Rev. Cell Dev. Biol.* **30,** 111–139
13. Yamada, S., Pokutta, S., Drees, F., Weis, W. I., and Nelson, W. J. (2005) Deconstructing the cadherin-catenin-actin complex. *Cell* **123,** 889–901
14. Shih, W., and Yamada, S. (2010) Myosin IIA dependent retrograde flow

drives 3D cell migration. *Biophys. J.* **98,** L29–L31
15. Duan, R., and Gallagher, P. J. (2009) Dependence of myoblast fusion on a cortical actin wall and nonmuscle myosin IIA. *Dev. Biol.* **325,** 374–385
16. Neco, P., Fernández-Peruchena, C., Navas, S., Gutiérrez, L. M., de Toledo, G. A., and Alés, E. (2008) Myosin II contributes to fusion pore expansion during exocytosis. *J. Biol. Chem.* **283,** 10949–10957
17. Charrasse, S., Comunale, F., Grumbach, Y., Poulat, F., Blangy, A., and Gauthier-Rouvière, C. (2006) RhoA GTPase regulates M-cadherin activity and myoblast fusion. *Mol. Biol. Cell* **17,** 749–759
18. Yamada, S., and Nelson, W. J. (2007) Localized zones of Rho and Rac activities drive initiation and expansion of epithelial cell-cell adhesion. *J. Cell Biol.* **178,** 517–527
19. Ridley, A. J. (2006) Rho GTPases and actin dynamics in membrane protrusions and vesicle trafficking. *Trends Cell Biol.* **16,** 522–529
20. Hakeda-Suzuki, S., Ng, J., Tzu, J., Dietzl, G., Sun, Y., Harms, M., Nardine, T., Luo, L., and Dickson, B. J. (2002) Rac function and regulation during *Drosophila* development. *Nature* **416,** 438–442
21. Haralalka, S., Shelton, C., Cartwright, H. N., Katzfey, E., Janzen, E., and Abmayr, S. M. (2011) Asymmetric Mbc, active Rac1 and F-actin foci in the fusion-competent myoblasts during myoblast fusion in *Drosophila*. *Development* **138,** 1551–1562
22. Vasyutina, E., Martarelli, B., Brakebusch, C., Wende, H., and Birchmeier, C. (2009) The small G-proteins Rac1 and Cdc42 are essential for myoblast fusion in the mouse. *Proc. Natl. Acad. Sci. U.S.A.* **106,** 8935–8940
23. Gruenbaum-Cohen, Y., Harel, I., Umansky, K. B., Tzahor, E., Snapper, S. B., Shilo, B. Z., and Schejter, E. D. (2012) The actin regulator N-WASp is required for muscle-cell fusion in mice. *Proc. Natl. Acad. Sci. U.S.A.* **109,** 11211–11216
24. Sens, K. L., Zhang, S., Jin, P., Duan, R., Zhang, G., Luo, F., Parachini, L., and Chen, E. H. (2010) An invasive podosome-like structure promotes fusion pore formation during myoblast fusion. *J. Cell Biol.* **191,** 1013–1027
25. Shilagardi, K., Li, S., Luo, F., Marikar, F., Duan, R., Jin, P., Kim, J. H., Murnen, K., and Chen, E. H. (2013) Actin-propelled invasive membrane protrusions promote fusogenic protein engagement during cell-cell fusion. *Science* **340,** 359–363
26. Champion, J. A., and Mitragotri, S. (2006) Role of target geometry in phagocytosis. *Proc. Natl. Acad. Sci. U.S.A.* **103,** 4930–4934
27. Gallop, J. L., Walrant, A., Cantley, L. C., and Kirschner, M. W. (2013) Phosphoinositides and membrane curvature switch the mode of actin polymerization via selective recruitment of toca-1 and Snx9. *Proc. Natl. Acad. Sci. U.S.A.* **110,** 7193–7198
28. Marcy, Y., Prost, J., Carlier, M. F., and Sykes, C. (2004) Forces generated during actin-based propulsion: a direct measurement by micromanipulation. *Proc. Natl. Acad. Sci. U.S.A.* **101,** 5992–5997
29. Römer, W., Pontani, L. L., Sorre, B., Rentero, C., Berland, L., Chambon, V., Lamaze, C., Bassereau, P., Sykes, C., Gaus, K., and Johannes, L. (2010) Actin dynamics drive membrane reorganization and scission in clathrin-independent endocytosis. *Cell* **140,** 540–553
30. Yao, L. H., Rao, Y., Bang, C., Kurilova, S., Varga, K., Wang, C. Y., Weller, B. D., Cho, W., Cheng, J., and Gong, L. W. (2013) Actin polymerization does not provide direct mechanical forces for vesicle fission during clathrin-mediated endocytosis. *J. Neurosci.* **33,** 15793–15798
31. Rougerie, P., Miskolci, V., and Cox, D. (2013) Generation of membrane structures during phagocytosis and chemotaxis of macrophages: role and regulation of the actin cytoskeleton. *Immunol. Rev.* **256,** 222–239
32. McNew, J. A., Weber, T., Parlati, F., Johnston, R. J., Melia, T. J., Söllner, T. H., and Rothman, J. E. (2000) Close is not enough: SNARE-dependent membrane fusion requires an active mechanism that transduces force to membrane anchors. *J. Cell Biol.* **150,** 105–117
33. Xu, H., Zick, M., Wickner, W. T., and Jun, Y. (2011) A lipid-anchored SNARE supports membrane fusion. *Proc. Natl. Acad. Sci. U.S.A.* **108,** 17325–17330
34. Harrison, O. J., Bahna, F., Katsamba, P. S., Jin, X., Brasch, J., Vendome, J., Ahlsen, G., Carroll, K. J., Price, S. R., Honig, B., and Shapiro, L. (2010) Two-step adhesive binding by classical cadherins. *Nat. Struct. Mol. Biol.* **17,** 348–357
35. Pérez-Vargas, J., Krey, T., Valansi, C., Avinoam, O., Haouz, A., Jamin, M., Raveh-Barak, H., Podbilewicz, B., and Rey, F. A. (2014) Structural basis of eukaryotic cell-cell fusion. *Cell* **157,** 407–419
36. Zeev-Ben-Mordehai, T., Vasishtan, D., Siebert, C. A., and Grünewald, K. (2014) The full-length cell-cell fusogen EFF-1 is monomeric and upright on the membrane. *Nat. Commun.* **5,** 3912
37. Drees, F., Pokutta, S., Yamada, S., Nelson, W. J., and Weis, W. I. (2005) α-Catenin is a molecular switch that binds E-cadherin-beta-catenin and regulates actin-filament assembly. *Cell* **123,** 903–915
38. Benjamin, J. M., Kwiatkowski, A. V., Yang, C., Korobova, F., Pokutta, S., Svitkina, T., Weis, W. I., and Nelson, W. J. (2010) αE-catenin regulates actin dynamics independently of cadherin-mediated cell-cell adhesion. *J. Cell Biol.* **189,** 339–352
39. Hansen, S. D., Kwiatkowski, A. V., Ouyang, C. Y., Liu, H., Pokutta, S., Watkins, S. C., Volkmann, N., Hanein, D., Weis, W. I., Mullins, R. D., and Nelson, W. J. (2013) αE-catenin actin-binding domain alters actin filament conformation and regulates binding of nucleation and disassembly factors. *Mol. Biol. Cell* **24,** 3710–3720